Turbomachinery blades damping by optimized shunted piezoelectric circuits

Stéphanie Livet, Manuel Collet, Marc Berthillier, Pierrick Jean, Jean-Marc Cote

Turbomachinery blades damping thanks to optimized shunted piezoelectric circuits

S. Livet[a], M. Collet[b], M. Berthillier[b], P. Jean[a] and J.M. Cote[b]

[a]Snecma, SAFRAN Group, Rond-Point René Ravaud - Réau, 77550 Moissy Cramayel, France;
[b]Femto-ST Institute, Applied Mechanics Dpt, 24 rue de l'Epitaphe, 25000 Besançon, France

ABSTRACT

Dynamics of gas-turbine blades are particularly aero-elastic coupling sensitive. These aerodynamic limits can be pushed away by adding extra damping to the structure in order to reach even better compressor performance. However nowadays design and manufacturing techniques in aero-mechanics are achieving their maximum of state-of-the-art.

As in many fields active control would solve easily this kind of instability. But the difficulty remains in the needed energy supply for actuators whereas these components are aimed to be bonded on rotating structures. The capacity of different auto-supplied devices using shunted piezoelectric circuits had been studied here to prevent turbomachine bladed from fluttering.

Before realizing the study on complex turbomachine geometries, the presented technique uses a numerical development thanks to a 1D Euler-Bernoulli beam model combining both mechanical and electrical coupling parameters. A second development thanks to a 3D model had been made using a commercial tool, Comsol software. These approximate models are used to optimize electrically the shunted piezoelectric element and its localization. The results, verified experimentally, let suppose that vibrations can be reduced significantly when shunted piezoelectric circuits are mounted on a real structure.

Keywords: Piezoelectricity, Semi-passive control, Damping, Turbomachine, Single-crystal, Negative capacitance

1. INTRODUCTION

Each new gas turbine generation require more and more demanding design techniques to correspond to the extreme environments and conditions of use. These have to be especially more and more light and efficient. The design methods for these machines imply an augmentation in volume and speed of the airflow to achieve such proportion of thrust/mass with the use of less components or lighter materials. The space between blade stages in compressors are also tighter with a lower number of stages. Consequently new compressors use extremely long profile blades, which rises the aerodynamics stresses.

The vibrations induced by the airflow in turbomachines are the cause of High Cycle Fatigue (HCF) and ask for regular and unexpected maintenance needs. The minimization of the vibration responses toward to the aerodynamics forces can reduce the HCF and by the way reduce significantly the deterioration phenomena and avoid high cost in repairing. The need of new solutions is trivial as most of the traditional solutions of minimization of HCF effects bring negative effect on the new effective designs, adding mass to the structure for instance. Moreover as the elderly concept engines may match the new expectations, after-design solutions have to be suggested and optimized easily without replacing any components.

The piezoelectric material present a new approach to vibration suppression in aeronautical structures[1,2] . They can be adapted to the creation of damping or control elements. Indeed when the electric current is applied to a piezoelectric material, a corresponding strain is produced within the material, which produces an electric voltage. Vibration damping of an elastic structure can be obtain by an piezoelectric actuator embedded into it

Further author information: (Send correspondence to S. Livet)
S. Livet: E-mail: stephanie.livet@univ-fcomte.fr, Telephone: +33 (0)3 81 66 60 37
M. Collet: E-mail: manuel.collet@univ-fcomte.fr, Telephone: +33 (0)3 81 66 67 28

and shunted to an electric resonant circuit adjusted to the mode to damp. The obtained damping depends on the type of electronic shunt and can be expressed directly taking into account the inherent structural damping coefficient or unstable phenomena as fluttering of the studied system.

In this paper, we present a simple Euler-Bernoulli beam model created on the Hamilton Principle[3,4] to be able to describe the studied phenomena and explain the role of the piezoelectric component in energy transfer between the schematically modeled blade structure and the electronic circuit. A more complex 3D model thanks to the Comsol software has been also achieved. First optimization guidelines have been highlighted to maximize the induced damping. An experiment has been settled to verify theoretical results on damping with a passive shunt the damping realized thanks to different piezoelectric shunt sticked onto steal beams of different length in order to be able to quantify the capability of passive control and check how much the piezoelectric system can likely dampen passively the structure.

2. EULER-BERNOULLI BEAM MODELING THANKS TO HAMILTON PRINCIPLE

2.1 Energy description

The Hamilton principle[5] is often used to construct Finite Element models. The beam model studied and exploited in this paper has been built on the same criteria. The variational principal can be written as $\delta \int_{t_o}^{t_1} (\mathcal{L} + \mathcal{W}) dt = 0$ with $\mathcal{L}$ Lagrangian term and $\mathcal{W}$ the virtual work of mechanical and electrical forces. $\mathcal{L} = T + H$ with T kinetic energy and H the enthalpy which worths by the IEEE definition[6] of the piezoelectricity, $H = U - E_i D_i$ with U the intern energy of the studied model.

2.1.1 Kinetic Energy expression

The kinetic energy expression can be expressed as $T = \frac{1}{2} \int_\Omega \rho \dot{u}_i \dot{u}_i d\Omega$, which leads to:$\delta T = \int_\Omega \rho \delta(\dot{u}_i) \dot{u}_i d\Omega$

2.1.2 Strain Energy Expression

For a piezoelectric element we can express the strain energy as: $H = \frac{1}{2} \int_\Omega {}^\dagger\{S\}\{T\} d\Omega - \frac{1}{2} \int_\Omega {}^\dagger\{E\}\{D\} d\Omega$

The piezoelectric equations of behaviour are:

$$\{T\} = \left[c^E\right]\{S\} - {}^\dagger[e]\{E\} \quad (1)$$

$$\{D\} = [e]\{S\} + \left[\varepsilon^S\right]\{E\} \quad (2)$$

where $\{T\}$ represents the stresses tensor, $\{S\}$ the strain tensor, $\{E\}$ the electric field, $\{D\}$ the electric displacement, $[c^E]$ the elastic coefficients at constant electric field $\{E\}$, $\{\varepsilon^S\}$ the dielectric coefficients at constant strain $\{S\}$, and $[e]$ the piezoelectric coupling coefficients.

We replace $\{T\}$ et $\{D\}$ by their respective expression in the Hamilton principle. Considering $\{S\}$ as a symmetric field, we find for H:

$$\begin{aligned} \int_{t_o}^{t_1} \delta H dt = & \int_\Omega \int_{t_o}^{t_1} \left[{}^\dagger\{\delta S\} \left[c^E\right]\{S\} \right] dt d\Omega - \int_\Omega \int_{t_o}^{t_1} \left[{}^\dagger\{\delta S\} {}^\dagger[e]\{E\} \right] dt d\Omega \\ & - \int_\Omega \int_{t_o}^{t_1} \left[{}^\dagger\{\delta E\}[e]\{S\} \right] dt d\Omega - \int_\Omega \int_{t_o}^{t_1} \left[{}^\dagger\{\delta E\} \left[\varepsilon^S\right]\{E\} \right] dt d\Omega \end{aligned} \quad (3)$$

2.2 Euler-Bernoulli Beam Model

2.2.1 Kinematic hypothesis of Euler-Bernoulli beam model

The initial 3D problem of elasticity is reduced to 1D problem. All functions (displacement, stresses...) depend on only one variable along the length of the beam, here noted x. We suppose also that the thickness and the width are small in comparison with the length and the beam is charged in its plane. The transverse strain is neglected in this model.

2.2.2 Strain expression in the case of a Euler-Bernoulli beam

Some articles show studies[7] with piezoelectric patches facing each other. These sandwich systems usually show a better efficiency of their system while the piezoelectric elements are perfectly bonded in opposite. In the case of aeronautical structure as blades, this position could not happen and that is why all our study is done with piezoelectric elements placed independently. For a beam with a piezoelectric element bond onto the surface the representative drawing of the model is the following:

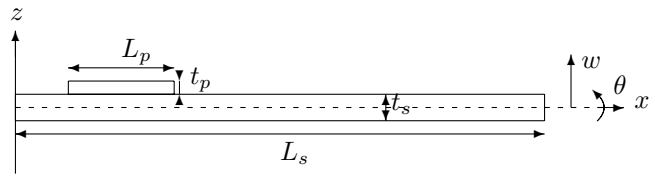

We consider the beam widths l_s et l_p respectively the one of the structure and of the piezoelectric. The variables w et θ correspond to the degrees of freedom of the beam.

By definition the termes ij of the strain tensor i in the hypothesis of small linear perturbations can be expressed as $S_{ij} = \frac{1}{2}\left(\frac{du_i}{dx_j} + \frac{du_j}{dx_i}\right)$. Further we will note $S_{ij} = S_i$ for $i = j$ and $2S_{ij} = S_{9-(i+j)}$ for $i \neq j$.

2.2.3 Piezoelectric coefficient correction

The characteristic coefficients of a piezoelectric are affected by the Euler-Bernoulli type modeling. The beam hypothesis implies a reduction of the number of piezoelectric parameters. We can consider the transverse efforts T_{xz} or T_5 neglected. The efforts T_2, T_3, T_4 et T_6 are considered equal to zero by the Euler-Bernoulli model.

For a piezoelectric element the equations can be written as:

$$\begin{Bmatrix} T_1 \\ T_2 \\ T_3 \\ T_4 \\ T_5 \\ T_6 \end{Bmatrix} = \begin{bmatrix} c_{11} & c_{12} & c_{13} & 0 & 0 & 0 \\ c_{12} & c_{22} & c_{13} & 0 & 0 & 0 \\ c_{13} & c_{13} & c_{33} & 0 & 0 & 0 \\ 0 & 0 & 0 & c_{44} & 0 & 0 \\ 0 & 0 & 0 & 0 & c_{44} & 0 \\ 0 & 0 & 0 & 0 & 0 & c_{66} \end{bmatrix}^E \begin{Bmatrix} S_1 \\ S_2 \\ S_3 \\ S_4 \\ S_5 \\ S_6 \end{Bmatrix} - \begin{bmatrix} 0 & 0 & e_{31} \\ 0 & 0 & e_{31} \\ 0 & 0 & e_{33} \\ 0 & e_{15} & 0 \\ e_{15} & 0 & 0 \\ 0 & 0 & 0 \end{bmatrix} \begin{Bmatrix} E_1 \\ E_2 \\ E_3 \end{Bmatrix} \tag{4}$$

Which gives us:

$$\begin{aligned} T_1 &= \left[c_{11}^E - \left(c_{33}^E c_{11}^E - {c_{13}^E}^2\right)^{-1}\left[c_{12}^E\left(c_{33}^E c_{12}^E - {c_{13}^E}^2\right) + {c_{13}^E}^2\left(c_{12}^E - c_{11}^E\right)\right]\right] S_1 \\ &+ \left[\left(c_{33}^E c_{11}^E - {c_{13}^E}^2\right)^{-1}\left[c_{12}^E\left(-c_{33}^E e_{31} + c_{13}^E e_{33}\right) + c_{13}^E\left(-c_{13}^E e_{31} + c_{11}^E e_{33}\right)\right] - e_{31}\right] E_3 \end{aligned} \tag{5}$$

By the same way we calculate the electrical equation part:

$$\begin{Bmatrix} D_1 \\ D_2 \\ D_3 \end{Bmatrix} = \begin{bmatrix} 0 & 0 & 0 & 0 & e_{15} & 0 \\ 0 & 0 & 0 & e_{15} & 0 & 0 \\ e_{31} & e_{31} & e_{33} & 0 & 0 & 0 \end{bmatrix} \begin{Bmatrix} S_1 \\ S_2 \\ S_3 \\ S_4 \\ S_5 \\ S_6 \end{Bmatrix} + \begin{bmatrix} \varepsilon_{11} & 0 & 0 \\ 0 & \varepsilon_{11} & 0 \\ 0 & 0 & \varepsilon_{33} \end{bmatrix}^S \begin{Bmatrix} E_1 \\ E_2 \\ E_3 \end{Bmatrix} \tag{6}$$

$$D_3 = e_{31}S_1 + e_{31}S_2 + e_{33}S_3 + \varepsilon_{33}E_3 \tag{7}$$

$$\begin{aligned} &= e_{31}S_1 - e_{31}\left(c_{33}^E c_{11}^E - {c_{13}^E}^2\right)^{-1}\left[\left(c_{33}^E c_{12}^E - {c_{13}^E}^2\right)S_1 + \left(c_{33}^E e_{31} + c_{13}^E e_{33}\right)E_3\right] \\ &- e_{33}\left({c_{13}^E}^2 - c_{11}^E c_{33}^E\right)^{-1}\left[c_{13}^E\left(c_{12}^E - c_{11}^E\right)S_1 + \left(-c_{13}^E e_{31} + c_{11}^E e_{33}\right)E_3\right] + \varepsilon_{33}E_3 \end{aligned} \tag{8}$$

when we write the system as in the manner developed by Maurini[8] , the new piezoelectric parameters are:

$$\{T_1\} = {c_{11}^E}^*\{S_1\} - e_{31}^*\{E_3\} \quad (9)$$

$$\{D_3\} = e_{31}^*\{S_1\} + {\varepsilon_{33}^S}^*\{E_3\} \quad (10)$$

$${c_{11}^E}^* = c_{11}^E + \left(c_{33}^E c_{11}^E - {c_{13}^E}^2\right)^{-1}\left[2c_{12}^E {c_{13}^E}^2 - \left({c_{12}^E}^2 c_{33}^E + {c_{13}^E}^2 c_{11}^E\right)\right] \quad (11)$$

$$e_{31}^* = e_{31} + \left(c_{33}^E c_{11}^E - {c_{13}^E}^2\right)^{-1}\left[-\left(c_{12}^E c_{33}^E - {c_{13}^E}^2\right)e_{31} + c_{13}^E\left(c_{12}^E - c_{11}^E\right)e_{33}\right] \quad (12)$$

$${\varepsilon_{33}^S}^* = \varepsilon_{33}^S + \left(c_{33}^E c_{11}^E - {c_{13}^E}^2\right)^{-1}\left[-e_{31}\left(c_{33}^E e_{31} + c_{13}^E e_{33}\right) + e_{33}\left(-c_{13}^E e_{31} + c_{11}^E e_{33}\right)\right] \quad (13)$$

In the case of a Euler-Bernoulli type resolution the displacement u_i which is defined as $u_1 = -z\frac{\partial w}{\partial x}$, $u_2 = 0$ et $u_3 = w(x,t)$ with $w(x,t)$ displacement of a point distant from the neutral fiber and $\frac{\partial w}{\partial x}(x,t) = -\theta(x,t)$ corresponding to the rotation of the section at the coordinate x. We obtain the strain $S_{11} = S_1 = \frac{\partial H_1}{\partial x} = z\frac{\partial^2 w}{\partial^2 x}$. We replace the obtained expressions into the Hamilton principle:

$$\begin{aligned}\int_{t_o}^{t_1}\delta H dt = & \int_\Omega\int_{t_o}^{t_1} {c_{11}^E}^* z^2 \frac{\partial^2\delta w}{dx^2}\frac{\partial^2 w}{\partial x^2}dtd\Omega - \int_\Omega\int_{t_o}^{t_1}\delta E_3 e_{31}^* z\frac{\partial^2 w}{\partial x^2}dtd\Omega \\ & - \int_\Omega\int_{t_o}^{t_1}\frac{\partial^2\delta w}{\partial x^2}e_{31}^* z E_3 dtd\Omega - \int_\Omega\int_{t_o}^{t_1}\delta E_3 {\epsilon_{33}^S}^* E_3 dtd\Omega \end{aligned} \quad (14)$$

2.2.4 Electrical model hypotheses

The electrical field can be defined as a potential gradient ϕ such as: $\vec{E} = -\vec{\nabla}\phi$. Then ϕ corresponds to the difference of electrical voltage between the two electrodes of the piezoelectric element. We can approximate the electrical field as constant through the thickness, which implies: $E_3 = -\frac{\phi}{dz}$ (z direction through the thickness of the piezoelectric element). We suppose that the inferior electrode is grounded: $\phi(x,y,z,t) = \phi(z,t)$ and we define z_p the height of the inferior electrode $z_p = \frac{t_s}{2}$. At the superior electrode we find $z = z_p + t_p = \frac{t_s}{2} + t_p$. and we have $\phi(z_p,t) = V(t) - V_0 = V(t)$, which gives us as solution $\phi = \frac{V}{t_p}(z - \frac{t_s}{2})$

$$E_3 = -\frac{\partial\phi}{\partial z} = -\frac{V}{t_p}z \quad (15)$$

In the framework of these hypotheses we find as piezoelectric strain expressions:

$$\begin{aligned}\int_{t_o}^{t_1}\delta H dt = & \int_\Omega\int_{t_o}^{t_1} {c_{11}^E}^* z^2 \frac{d^2\delta w}{dx^2}\frac{\partial^2 w}{\partial x^2}dtd\Omega + \int_\Omega\int_{t_o}^{t_1}\delta V\frac{e_{31}^* z}{t_p}\frac{\partial^2 w}{\partial x^2}dtd\Omega \\ & + \int_\Omega\int_{t_o}^{t_1}\frac{\partial^2\delta w}{\partial x^2}\frac{e_{31}^* z}{t_p}V dtd\Omega - \int_\Omega\int_{t_o}^{t_1}\delta V\frac{{\epsilon_{33}^S}^*}{t_p^2}V dtd\Omega \end{aligned} \quad (16)$$

3. FINITE ELEMENT DECOMPOSITION

3.1 1D Finite Element model

We replace, in the strain energy expression, the precedent displacement as a polynomial function and split up into two distinct functions independent respectively from time and space parameters $w(x,t) = W(x)\eta(t)$. We can distinguish three terms in the strain energy expression[9] : a pure mechanical parameter δH_m, two electro-mechanical coupling parameters δH_{em} et δH_{me} and an electrical parameter δH_e.

Let i be the index summing the structural elements s and the piezoelectric ones p.

$$\delta H_m = {}^\dagger\{\delta\eta(t)\}\int_{x=0}^{L_i} E_i I_i\ {}^\dagger[W''(x)][W''(x)]\ dx\ \{\eta(t)\} \quad (17)$$

$$\delta H_{me} = \delta H_{em} = -\delta V \int_{x=0}^{L_p} \frac{l_p(t_s+t_p)}{2} e_{31}^* [W''(x)]\ dx\ \{\eta(t)\} \quad \text{and} \quad \delta H_e = -\frac{l_p L_p}{t_p} \epsilon_{33}^{S\,*} \delta V V$$

The elementary stiffness and mass matrices for the system {beam+piezoelectric} can be calculated from the strain energy expression.

3.1.1 Stiffness Matrix

The elementary stiffness matrix can be written as equation 18 with I structural inertia developed in Appendix B.

$$K^e = \begin{bmatrix} K_{mm}^e & K_{me}^e \\ K_{em}^e & K_{ee}^e \end{bmatrix} = \begin{bmatrix} c_{11}^{E\,*} I L_e\ {}^\dagger[W''][W''] & \frac{l_p(t_s+t_p)}{2}\ e_{31}^*\ {}^\dagger[0,-1,0,1] \\ \frac{l_p(t_s+t_p)}{2}\ e_{31}^*\ [0,-1,0,1] & -\frac{l_p L_p}{t_p}\ \varepsilon_{33}^{S\,*} \end{bmatrix} \tag{18}$$

We note the piezoelectric characteristics: $\alpha = \frac{l_p(t_s+t_p)}{2}\ e_{31}^*$ coupling coefficient and $C_p^S = \frac{l_p L_p}{t_p}\ \varepsilon_{33}^{S\,*}$ the inherent capacity at constant strain of the piezoelectric element of length L_e.

3.1.2 Mass Matrix

The mass matrix M of the system comes from the kinetic expression T previously calculated and using the same methodology as before for the stiffness matrix. $\delta T = -\rho_i \int_{\Omega_i} \delta u_i \ddot{u}_i d\Omega$ but $u_1 \approx 0$, $u_2 = z\dfrac{\partial w}{\partial x}$ et $u_3 = w$.

The influence of the inertia is neglected on the kinetic energy.

$$\delta T = -\rho_i S_i\ {}^\dagger\{\delta\eta(t)\} \int_{x=0}^{L_i} {}^\dagger[W(x)][W(x)]\ dx\ \{\ddot{\eta}(t)\} \tag{19}$$

From the expression 19, we drag out the elementary matrix $[M^e]$:

$$[M^e] = \rho_i I_i \int_{x=0}^{L_i} {}^\dagger[W'(x)][W'(x)]\ dx \tag{20}$$

To complete the study the pure mechanical matrices of a Euler-Bernoulli model are recalled in Appendix C.

3.2 FE electromechanical system

For a FE system the assembly of the whole system linked to a shunt circuit in dynamic and in the case of a electrical shunt realized between the electrodes, we have for a piezoelectrical mechanical system the following relation written for one element:

$$[M_{mm}]\{\ddot{w}\} + [G_{mm}]\{\dot{w}\} + [K_{mm}]\{w\} + [K_{me}]\{V\} = \{F\} \tag{21}$$
$$[K_{em}]\{w\} - [K_{ee}]\{V\} = -\{q\} \tag{22}$$

In the case of a shunt with a Z impedance, $V = -sZq$ with s Laplace coefficient.

$$[M_{mm}]\{\ddot{w}\} + [G_{mm}]\{\dot{w}\} + \left([K_{mm}] + [K_{me}][K_{ee}]^{-1}[K_{em}]\right)\{w\} + [K_{me}][K_{ee}]^{-1}\{q\} = \{F\} \tag{23}$$
$$sZ[K_{ee}]\{q\} + \{q\} + [K_{em}]\{w\} = 0 \tag{24}$$

We can notice that in the case of short circuit $V = 0$ and we return to a purely mechanical system:

$$[M_{mm}]\{\ddot{w}\} + [G_{mm}]\{\dot{w}\} + [K_{mm}]\{w\} = \{F\} \tag{25}$$

and in the case of open circuit $q = 0$:

$$[M_{mm}]\{\ddot{w}\} + [G_{mm}]\{\dot{w}\} + \left([K_{mm}] + [K_{me}][K_{ee}]^{-1}[K_{em}]\right)\{w\} = \{F\} \tag{26}$$

The stiffness value increases from a parameter $K'_{mm} = [K_{me}][K_{ee}]^{-1}[K_{em}]$ linked to the electromechanical (the coupling α) and electric (the inherent capacity C_p) parameters. This frequency gap between open and short circuit is regularly used as a optimization criteria[10] .

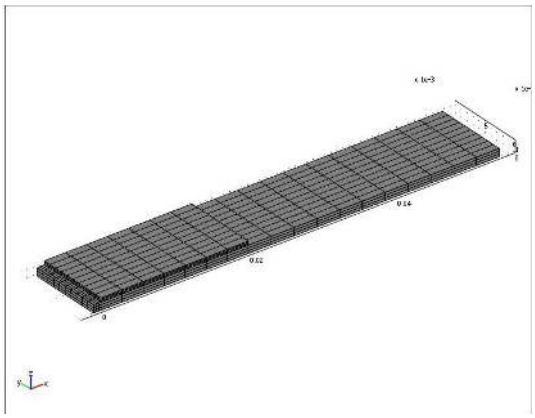

Figure 1. Picture from 3D Comsol model

3.3 3D modeling and state space system resolution

The 3D model represented in figure 1 is realized with the Comsol myltiphysics software.

The FE electromechanical system from equation 3 is firstly reduced by the methodology developed by Collet[11] . This methodology condensation allows a more accurate computation of the piezoelectric impedances. The induced matrices are exploited to create the final model in Matlab. To connect the FE model to shunt circuit we write the system as a Linear Time Invariant (LTI) System described just below:

$$\left\{ \begin{array}{rcl} \dot{N} & = & AN + BE \\ S & = & CN + DE \end{array} \right. \tag{27}$$

We define the observability variable with all the displacements $x = \phi\eta$ with ϕ functions based on the condensation methodology[11] :

$$N = \left\{ \begin{array}{c} \eta \\ \dot{\eta} \end{array} \right\} \tag{28}$$

The input of the system:

$$E = \left\{ \begin{array}{c} V \\ F \end{array} \right\} \tag{29}$$

The output with $w = C_{d1}x$ deflection of the beam tip:

$$S = \left\{ \begin{array}{c} q \\ w \end{array} \right\} \tag{30}$$

We write the initial system as a linear state problem with M, K and G respectively Mass, Stiffness, Damping Matrices:

$$\left\{ \begin{array}{c} \dot{x} \\ \ddot{x} \end{array} \right\} = \left[\begin{array}{cc} 0 & I \\ -M^{-1}K & -M^{-1}G \end{array} \right] \left\{ \begin{array}{c} x \\ \dot{x} \end{array} \right\} + \left[\begin{array}{cc} 0 & 0 \\ M^{-1}F_{u1} & M^{-1}F_{u2} \end{array} \right] E \tag{31}$$

$$S = \left[\begin{array}{cc} C_{d1} & 0 \\ C_{d2} & 0 \end{array} \right] \left\{ \begin{array}{c} x \\ \dot{x} \end{array} \right\} + [D_d \; 0] \, E \tag{32}$$

In the case of a shunted piezoelectric with a electrical circuit of Z impedance. We have also the relation $V = -Zsq$ with s the Laplace operator. Here we connected to the piezoelectric a resistive R_s and negative capacity C_s in series and $Z = R_s s + 1/C_s$ and $q = C_{d1}x + D_d V$ as in our experimental work (developed in section 4.3) but the method can be used for many other kinds of electrical circuits.

$$V = -(R_s s + 1/C_s)(C_{d1}\eta + D_d V) = -R_s C_{d1}\dot{\eta} - R_s D_d \dot{V} - C_s^{-1} C_{d1}\eta - 1/C_s D_d V \tag{33}$$

Hence $\dot{V} = -C_{d1}D_d^{-1}\dot{\eta} - (C_s^{-1}C_{d1})(R_sD_d)^{-1}\eta - (C_s^{-1}D_d + 1)(R_sD_d)^{-1}V$;

$$\left\{ \begin{array}{rcccccc} \dot{N} & = & A & N & + & B & E \\ \dot{V} & = & \left[-C_{d1}D_d^{-1} \;\; -(C_s^{-1}C_{d1})(R_sD_d)^{-1}\right] & N & + & \left[-(C_s^{-1}D_d+1)(R_sD_d)^{-1} \; 0\right] & E \end{array} \right. \tag{34}$$

$$\left\{ \begin{array}{rcccccc} \dot{N} & = & A & N & + & B & E \\ \dot{V} & = & C' & N & + & [Dd' \; 0] & E \end{array} \right. \tag{35}$$

We can write the new linear state system taking into account the electronic circuit with a new observation parameter $N' = \left\{ \begin{array}{c} N \\ V \end{array} \right\}$, entry F and output $S' = \left\{ \begin{array}{c} V \\ w \end{array} \right\}$.

$$\dot{N'} = \left[\begin{array}{cc} A & M^{-1}F_{u1} \\ C' & D'_d \end{array} \right] N' + M^{-1}F_{u2} \; F \tag{36}$$

$$S' = \left[\begin{array}{ccc} C_{d2} & 0 & 0 \\ 0 & 0 & 0 \\ 0 & 0 & 1 \end{array} \right] N' + 0 \; F \tag{37}$$

3.4 First study of optimal piezoelectric damping with a resistive shunt

Many studies[5,12] have detailed some damping optimization with several electronic shunts involving inductive, resistive, capacitive or switching components. In this paper we focused on the capability of passive damping on structure as it is very difficult, if not impossible, to supply the electric devices in aeronautical structures. Therefore we glanced preferentially at the mechanical coupling carried out between the structure and the piezoelectric element and which plays a very high role in passive control. A first study has been realized to observe the evolution of the maximal damping ratio obtained by a purely resistive shunt as a function of the length of the piezoelectric element from the resolution of sections 3.2 and 3.3 for an electric impedance $Z = R$. The piezoelectric is kept at the base of the root of the cantilever beam and we took here a 55mm long-10mm wide-1mm thick beam. The piezoelectric has the same width as the beam and is 0.5mm thick. These values correspond to the values used later in the experimental work (section 4.1). The simulations are realized for a piezoelectric element from Saint Gobain Quartz (P1 94).

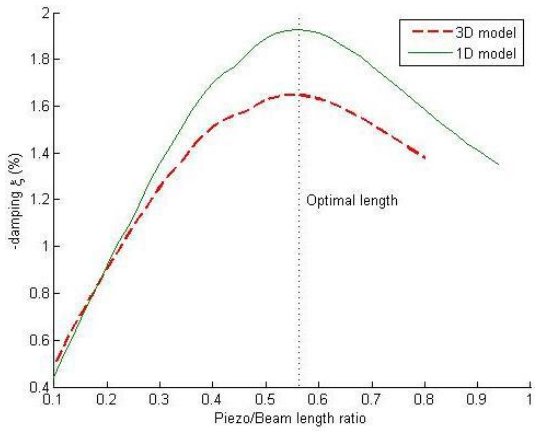

Figure 2. Comparison of the evolution of the length of the piezoelectric element modeled in 1D and 3D

In this particular case we observe that the maximum of damping, calculated at an optimal resistance for each length ratio, is obtained for a piezoelectric length around the middle of the beam (fig. 2). At the same time of the decreasing of the damping ratio, the added mass on the second part of the beam, where the beam strain is the weaker, makes also the eigen frequency of the first mode diminish.

4. EXPERIMENTAL RESULTS

4.1 Experimental protocol

A steel beam has been used to check the modeling by the Euler-Bernoulli and 3D Comsol model (fig. 3). Each time we kept constant the size of the piezoelectric (20mm x10mm x0.5mm) to be able to compare and evaluate the extra damping in function of different relative lengths (55-70-90mm x10mm x1mm) of the host structure. The piezoelectric element is bonded close to the cantilever beam root (2mm distance) to retrieve good damping results for the first bending mode as the strain is then maximum, the piezoelectric being sensitive to the beam strain.

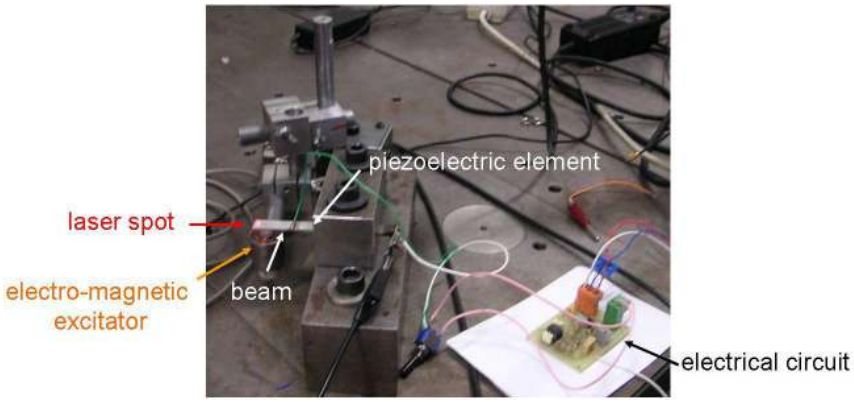

Figure 3. Picture of the experimental assembly

The beam is excited by an electro-magnetic generator with a residual magnetic field to be able to excite the metal beam at distance. The damping on the first mode from a white noise is measured by a laser velocimetre and acquired by a PC with Siglab software.

4.2 Resistive shunt

4.2.1 Damping influence from the length ratio of piezoelectric patches

We desired to quantify the capability of damping impact thanks to a resistive shunt and by this way evaluate the maximum of coupling between the piezoelectric and the beam. When we make the resistance shunt on the piezoelectric patch vary from 0 (short circuit) to $+\infty$ (open circuit). This phenomena can be explained by the direct impact which the resistance has onto the stiffness of the whole structure {piezo+beam} as explained in section 3.2. Increasing the resistance implies so an increase of the damping ratio at the beginning and a decrease after passing by an optimum, while the frequency keeps increasing.

A summary table 1 of all the experiments is drew up for the first mode.

	55mm beam	70mm beam	90mm beam
Short-circuit frequency	360.3 Hz	210.0 Hz	121.4 Hz
Open-circuit frequency	366.5 Hz	212.7 Hz	122.7 Hz
Structural damping (%)	−0.1768	−0.1295	−0.1376
Maximal damping at R_{opt} (%)	−0.9764	−0.744	−0.654
δ damping at R_{opt} (%)	−0.80	−0.61	−0.52
δ magnitude damping	−18 dB	−13 dB	−12 dB

Table 1. Passive damping results from experiments

4.2.2 Damping impact due to piezoelectric material type

Two different types of piezoelectric material have been also tested during the experimental studies. Keeping the same size of material, we wanted to test the capability of the new material PMN-33PT from TRS Technology in comparison with PZTs (Appendix A)[13] . The capabilities of such a material were already proved in vibration absorption[14] . The PMN-33PT is a single crystal material and is a relatively softer piezoelectric element, which induce lower eigen frequencies of the whole structure. It has so less impact on the host behaviour and deflection of the beam. Moreover it has also better coupling coefficients. For a 55mm beam we observe experimentally a damping gain of about 100% with a PMN-33PT in comparison to the used PZT in section 4.2.1 . The extra damping ξ on the structure reaches about 2%, which corresponds to an amplitude loss of $-25dB$ (fig. 4).

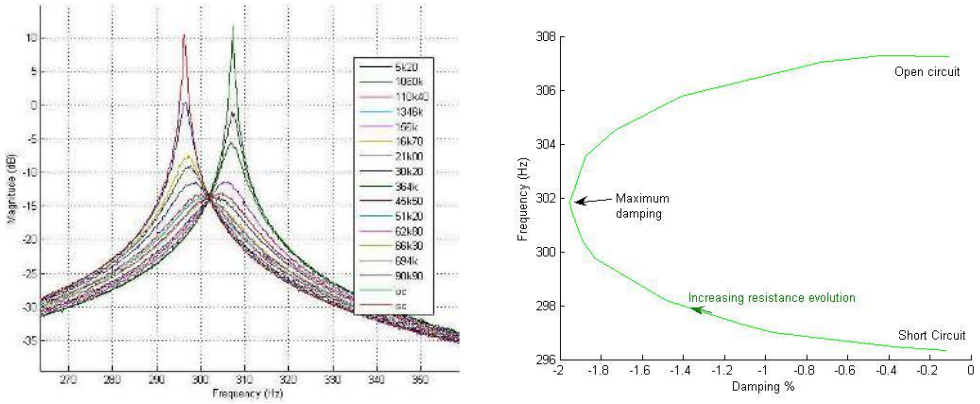

Figure 4. Bode and Evans diagrams of a 55mm beam with a PMN-33PT at different resistive shunt

4.2.3 Correlation with theoretical modeling

Though the whole experimental work has been realized with a PZT, P1 94 from Saint Gobain Quartz, we choose to move the piezoelectric characteristics closer to the ones of a P1 91 from Appendix A. Indeed we can hypothetically suppose that the PZT may have lost of its polarization during the cure needed to bond on the steel beam (80°C) thanks to a conductive glue (H20E of Epotek).

Beam length	55mm		70mm		90mm	
Model type	1D	3D	1D	3D	1D	3D
Short-circuit frequency	361.0 Hz	354.9 Hz	213.9 Hz	211.0 Hz	124.0 Hz	122.7 Hz
Experimental relative error (%)	0.194	−1.50	1.86	0.48	2.1	1.07
Open-circuit frequency	367.0 Hz	361 Hz	216.9 Hz	213.9 Hz	125.4 Hz	124.1 Hz
Structural damping (%)	−0.18	−0.18	−0.13	−0.13	−0.14	−0.14
Maximal damping at R_{opt} (%)	−0.995	−1.00	−0.832	−0.811	−0.655	−0.666
Experimental relative error (%)	1.90	2.4	11.8	9.0	0.153	1.83

Table 2. Passive damping results from 1D and 3D theory

The relative error which can be read in table 2 on the expected theoretically damping is rather small. We pointed out that most of the frequencies are overestimated which can be explained by the fact that the glue is not taken into account in the different models. In consequence we observe that the glue may add some mass on the structure but seems to have a poor impact on the damping ratio.

4.3 Negative capacitance shunt

To increase the efficiency of the damping due to Joule Effect and heat consummation through the resistance, we studied also the possibility to prevent the energy from getting stocked into the inherent capacity. The study

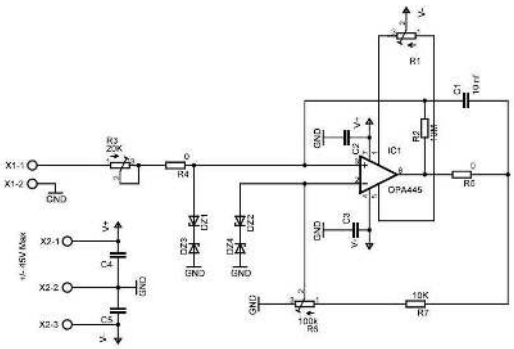

Figure 5. Electronic negative capacity diagram

such a system (developed in 3D in section 3.3) correspond to the one brought by an integral force feedback[10] . Therefore a negative capacity C_s represented by the figure 5 is added into the electrical circuit.

The device works as an equivalent negative capacity $C_{eq} = -\frac{R_7+\gamma R_8}{(1-\gamma)R_8}C_1$ for frequencies above $\frac{1}{R_3C_1}$. It can be tuned thanks to γ through the potentiometer R_8 variable from 0 to $20k\Omega$, which explains the lines break on the evans diagram (fig. 6). We can then observe the very high degree of damping thanks to this system in figure 6, where resistive damping evans loops are represented for different values of negative capacities. With a simple PZT bond on a 55mm long beam, we gain more than 4% of damping and $-30dB$ in magnitude on the first mode just before the instability, in comparison to 1% of damping and $-18dB$ in magnitude with a simple resitive shunt (section 4.2.1). Indeed the system remains stable for negative capacities below the capacity at contant stress C_p^T. This instability corresponds to the highest pick visible on the bode diagram on figure 6 traced for a capacity C_s just above $-C_p^T$.

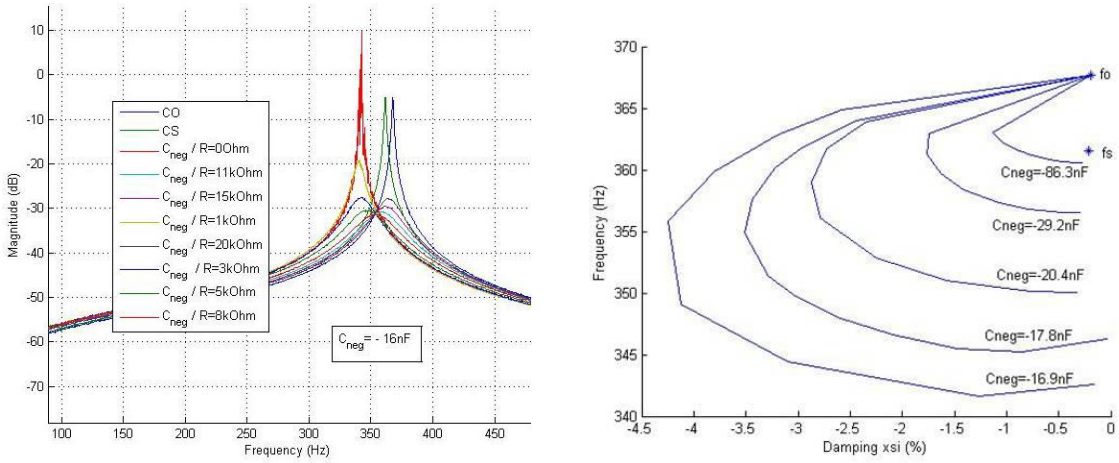

Figure 6. Bode and Evans diagrams of a 55mm beam with a PZT at different negative capacity and resistive shunt

5. CONCLUSION

With the arrival of new designs of engine components and the severe requirements which they have to follow, innovation techniques to control blade vibrations in gas turbines have to be considered and studied. The critical vibration modes are associated to the aspect ratio of blades. A high ratio makes the blade considered as a beam with a typical response of low orders as bending or torsion modes. The model presented here corresponds to these systems. However the characteristics of blade vibrations with a low aspect ratio are closer to a shell model and present more complex modes. Induced fluid-structure coupling vibrations present in this last case have a very

low inherent structural damping so this technique of damping with a piezoelectric shunt can be very interesting too if applied here.

The potential of such a damping on a turbomachine is very interesting in theory as shown by the theoretical models presented here and validated by the experimental work. Indeed the gain obtained experimentally is as good as expected from a two-degree-of-freedom model (Euler-Bernoulli Beam) suggested by the variational principle as well as from the 3D Comsol model. The purely passive method seems so to conclude experimentally to a very large damping addition (almost 2% with a PMN-33PT and about -25dB only with a resistance), which is actually globaly efficient enough to prevent instability from aerodynamics coupling to occur. The negative capacity circuit presents better results, however it can present some difficulties to be adjusted correctly. The passive control remains also always stable and can be adapted more easily to a muti-modal damping with several piezoelectric element correctly adjusted and wisely localised on the structure. For a complex blade geometry, the theoretical model is certainly to crude to represent fairly enough an hypothetic experimental model and will be soon enriched, the experimental perspectives being to be able to implement a passive control on fan blades or disk-assemblies[15] . The aim of our next studies will be to prevent fluttering phenomena from appearing and to push as far as possible the aerodynamics limits within the material resistance frontiers thanks to the optimisation presmiss guidelines.

APPENDIX A. PIEZOELECTRIC PROPERTIES

$c^E(10^9 N.m^{-2})$	c_{11}^E	c_{12}^E	c_{13}^E	c_{33}^E	c_{44}^E	c_{66}^E
P1 94	153.1	104.9	103.9	136.9	37.5	24.1
P1 91	120.9	76.3	73.1	112.6	33.6	22.3
PMN-33PT	115	103	102	103	69	66

Table 3. Modulus parameters

$e(C.m^2)$	e_{31}	e_{33}	e_{15}
P1 94	-12.4	26.2	20.8
P1 91	-4.9	21.4	17.1
PMN-33PT	-3.9	20.3	10.1

$\varepsilon(\varepsilon_0)$	ε_{11}^S	ε_{33}^S
P1 94	2710	2230
P1 91	1820	1461
PMN-33PT	1434	680

Table 4. Piezoelectric coupling and permittivity coefficients

APPENDIX B. INERTIA CALCULATION

The inertia I_{xy} is defined as $I_{xy} = \int_z \int_y z^2 dA$ with $dA = dzdy$.

For the structure $I_s = \int_{z=-\frac{t_s}{2}}^{\frac{t_s}{2}} \int_{y=-\frac{l_s}{2}}^{\frac{l_s}{2}} z^2 dA = \dfrac{l_s t_s^3}{12}$.

For the piezoelectric element $I_p = \int_{z=\frac{t_s}{2}}^{\frac{t_s}{2}+tp} \int_{y=-\frac{l_p}{2}}^{\frac{l_p}{2}} z^2 dA = \dfrac{l_p}{3} t_p \left(\dfrac{3t_s^2}{4} + \dfrac{3t_p t_s}{2} + t_p^2 \right)$.

APPENDIX C. EULER-BERNOULLI COEFFICIENTS

The Hamilton principle leads naturally to the pure mechanical results for a Euler-Bernoulli beam that we find out developing the term $^{\dagger}[W^{''}][W^{''}]$ with $W(x)$ expressed as with $\{w_1,\theta_1\}$ and $\{w_2,\theta_2\}$ respectively degrees of freedom of nodes at the coordinate x_1 and x_2:

$$W(x) = \left[1 - \frac{3}{L_e^2}x^2 + \frac{2}{L_e^3}x^3\right] w_1 + \left[x + \frac{1}{L_e}x^2 + \frac{1}{L_e^2}x^3\right] \theta_1 + \left[\frac{3}{L_e^2}x^2 - \frac{2}{L_e^3}x^3\right] w_2 + \left[-\frac{1}{L_e}x^2 + \frac{1}{L_e^2}x^3\right] \theta_2$$

Stiffness matrix	for a determined-determined element beam	for a determined-free element
K^e_{mm}	$\frac{EI}{L^3}\begin{pmatrix} 12 & 6L_e & -12 & 6L_e \\ 6L_e & 4L_e^2 & -6L_e & 2L_e^2 \\ -12 & -6L_e & 12 & -6L \\ 6L_e & 2L_e^2 & -6L_e & 4L_e^2 \end{pmatrix}$	$\frac{EI}{L^3}\begin{pmatrix} 3 & 3L_e & -3 & 0 \\ 3L_e & 3L_e^2 & -3L_e & 0 \\ -3 & -3L_e & 3 & 0 \\ 0 & 0 & 0 & 0 \end{pmatrix}$
Mass Matrix	for a determined-determined element beam	for a determined-free element
M^e_{mm}	$\frac{\rho V}{420}\begin{pmatrix} 156 & 22L_e & 54 & -13L_e \\ 22L_e & 4L_e^2 & 13L_e & -3L_e^2 \\ 54 & 13L_e & 156 & -22L_e \\ -13L_e & -3L_e^2 & -22L_e & 4L_e^2 \end{pmatrix}$	$\frac{\rho V}{420}\begin{pmatrix} 204 & 36L & 58.5 & 0 \\ 36L & 8L^2 & 16.5L & 0 \\ 58.5 & 16.5L & 99 & 0 \\ 0 & 0 & 0 & 0 \end{pmatrix}$

REFERENCES

[1] C. J. Cross and S. Fleeter, "Shunted piezoelectrics for passive control of turbomachine blading flow-induced vibrations," *Smart Material Structures* **11**, pp. 239–248, Apr. 2002.

[2] A. Agneni, F. Mastroddi, and G. M. Polli, "Shunted piezoelectric patches in elastic and aeroelastic vibrations," *Computers and Structures* , pp. 91–105, 2003.

[3] V. Piefort, *Finite Element Modeling of Piezoelectric Active Structures*. PhD thesis, Université Libre de Bruxelles, 2001.

[4] H. F. Tiersten, *Linear Piezoelectric Plate Vibration, Elements of the Linear Theory of Piezoelectricity and the Vibrations of Piezoelectric Plates*, Plenum Press, New York, 1969.

[5] A. Benjeddou, "Advances in piezoelectric finite element modeling of adaptive structural elements: a survey," *Computers and Structures* **76**, pp. 347–363, 2000.

[6] *IEEE Standard on Piezoelectricity*, ANSI/IEEE Std 176-1987, 1988.

[7] C. Maurini, J. Pouget, and F. dell'Isola, "Extension of the euler-bernoulli model of piezoelectric laminates to include 3d effect via a mixed approach," *Journal Computer and Structures* **84**, pp. 1438–1458, 2006.

[8] C. Maurini, *Piezoelectric composites for distributed passive electric control: beam modeling, modal analysis, and experimental implementation*. PhD thesis, Université Paris 6, 2005.

[9] C. K. Lee, "Theory of laminated piezoelectric plates for the design of distributed sensors/actuators. part i: Governing equations and reciprocal relationships," *Journal of the Acoustical Society of America* **87**, pp. 1144–1158, 1990.

[10] P. Monnier, M. Collet, and J. Piranda, "Definition of mechanical design parameters to optimize efficiency of integral force feedback," *Structural Control and health monitoring* **12**, pp. 65–89, Oct. 2004.

[11] M. Collet, "Modal synthesis and dynamical condensation methods for accurate piezoelectric systems impedance computation," *Journal of Intelligent Material Systems and Structures* , accepted for publication in 2008.

[12] G. Lesieutre, "Vibration damping and control using shunted piezoelectric materials," *The Shock and Vibration Digest* **30**, pp. 187–195, May 1998.

[13] V. H. Cao, V. Schmidt, W. Cao, Z. Rui, and H. Luo, "Elastic, piezoelectric and dielectric properties," *Journal of Applied Physics* **96**, pp. 549–554, 2004.

[14] R. Rusovici, J. J. Dosch, and G. A. Lesieutre, "Design of a single-crystal piezoceramic vibration," *Journal of Intelligent Material Systems and Structures* **13**, pp. 705–712, Nov. 2002.

[15] G. S. Agnes, "Piezoelectric coupling of bladed-disk assemblies," in *Proc. SPIE Vol. 3672, p. 94-103, Smart Structures and Materials 1999: Passive Damping and Isolation*, T. T. Hyde, ed., pp. 94–103, June 1999.